Pores and Ridges: High-Resolution Fingerprint Matching Using Level 3 Features

Anil K. Jain, *Fellow, IEEE*, Yi Chen, *Student Member, IEEE*, and
Meltem Demirkus, *Student Member, IEEE*

Abstract—Fingerprint friction ridge details are generally described in a hierarchical order at three different levels, namely, Level 1 (pattern), Level 2 (minutia points), and Level 3 (pores and ridge contours). Although latent print examiners frequently take advantage of Level 3 features to assist in identification, Automated Fingerprint Identification Systems (AFIS) currently rely only on Level 1 and Level 2 features. In fact, the Federal Bureau of Investigation's (FBI) standard of fingerprint resolution for AFIS is 500 pixels per inch (ppi), which is inadequate for capturing Level 3 features, such as pores. With the advances in fingerprint sensing technology, many sensors are now equipped with dual resolution (500 ppi/1,000 ppi) scanning capability. However, increasing the scan resolution alone does not necessarily provide any performance improvement in fingerprint matching, unless an extended feature set is utilized. As a result, a systematic study to determine how much performance gain one can achieve by introducing Level 3 features in AFIS is highly desired. We propose a hierarchical matching system that utilizes features at all the three levels extracted from 1,000 ppi fingerprint scans. Level 3 features, including pores and ridge contours, are automatically extracted using Gabor filters and wavelet transform and are locally matched using the Iterative Closest Point (ICP) algorithm. Our experiments show that Level 3 features carry significant discriminatory information. There is a relative reduction of 20 percent in the equal error rate (EER) of the matching system when Level 3 features are employed in combination with Level 1 and 2 features. This significant performance gain is consistently observed across various quality fingerprint images.

Index Terms—Fingerprint recognition, high-resolution fingerprints, minutia, Level 3 features, extended feature set, pores, ridge contours, hierarchical matching.

---

1 INTRODUCTION

FINGERPRINT identification is based on two properties, namely, uniqueness and permanence. It has been suggested that no two individuals (including identical twins) have the exact same fingerprints. It has also been claimed that the fingerprint of an individual does not change throughout the lifetime, with the exception of a significant injury to the finger that creates a permanent scar. In an article published in *Nature* in 1888 [1], Galton stated that "*personal characteristics exist in much more minute particulars... Perhaps the most beautiful and characteristic of all superficial marks are the small furrows with the intervening ridges and their pores that are disposed in a singularly complex yet even order on the under surfaces of the hands and the feet.*" The early work of Galton and Henry [2] forms the basis of the fingerprint identification approach as practiced today, especially in the forensic community.

Characteristic fingerprint features are generally categorized into three levels. Level 1 features, or patterns, are the macro details of the fingerprint such as ridge flow and pattern type. Level 2 features, or points, refer to the Galton characteristics or minutiae, such as ridge bifurcations and endings. Level 3 features, or shape, include all dimensional attributes of the ridge such as ridge path deviation, width,

shape, pores, edge contour, incipient ridges, breaks, creases, scars, and other permanent details (see Fig. 1). Statistical analysis has shown that Level 1 features, though not unique, are useful for fingerprint classification (e.g., into whorl, left loop, right loop, and arch classes), while Level 2 features have sufficient discriminating power to establish the individuality of fingerprints [5], [6]. Similarly, Level 3 features are also claimed to be permanent, immutable, and unique according to the forensic experts, and if properly utilized, can provide discriminatory information for human identification [7], [8].

In latent (partial) print examination, both Level 2 and Level 3 features play important roles in providing quantitative as well as qualitative information for identification. As stated by latent print examiner Ashbaugh, "*It is not the points, but what's in between the points that matters*" [7]. Unfortunately, commercial Automated Fingerprint Identification Systems (AFIS) barely utilize Level 3 features. This is because, in order to extract fine and detailed Level 3 features, we need high-resolution ($\geq$ 1,000 pixels per inch (ppi)) images. Since current AFIS systems are based only on 500 ppi images, the matchers used in these systems have been developed primarily based on Level 1 and Level 2 features.

With the advent of high-resolution fingerprint sensors and growing demand and requirements for accurate and robust latent print examination, there is a need to quantify the discriminating power of Level 3 features. In the 2005 ANSI/NIST fingerprint standard update workshop [9], the Scientific Working Group on Friction Ridge Analysis, Study and Technology (SWGFAST) [10] proposed a minimum scanning resolution of 1,000 ppi for latent, tenprint, and palm print images and the inclusion of Level 3 fingerprint features in the FBI standard. This proposal was strongly

---

● *The authors are with the Department of Computer Science and Engineering, Michigan State University, 3115 Engineering Building, East Lansing, MI 48824-1226.*
E-mail: {jain, chenyi1, demirkus}@cse.msu.edu.

LEVEL 1 FEATURES

ARCH   TENTED ARCH   LEFT LOOP   RIGHT LOOP   DOUBLE LOOP   WHORL

LEVEL 2 FEATURES

LINE-UNIT   LINE-FRAGMENT   ENDING   BIFURCATION   EYE   HOOK

LEVEL 3 FEATURES

PORES   LINE SHAPE   INCIPIENT RIDGES   CREASES   WARTS   SCARS
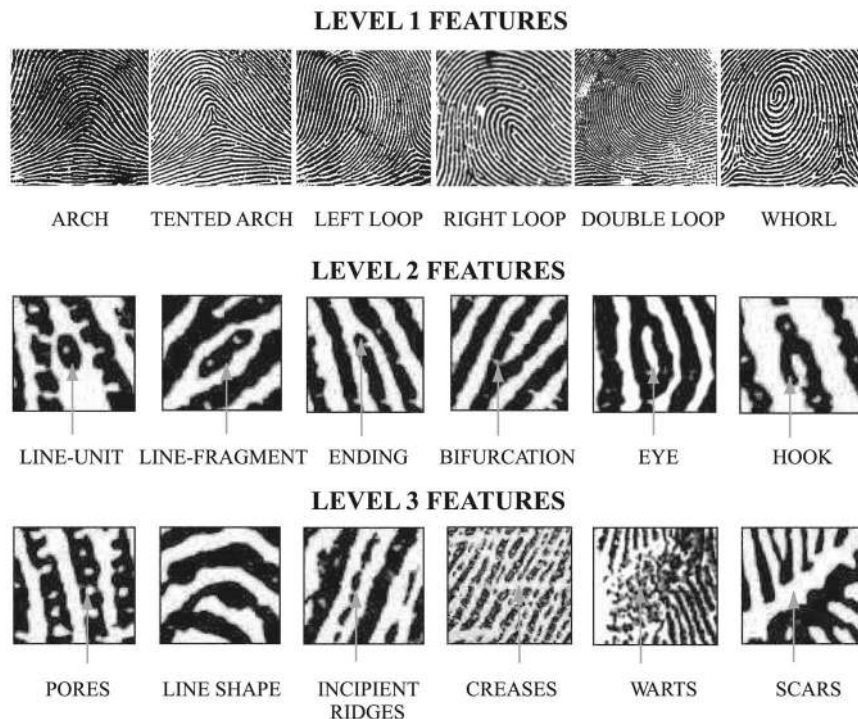
Fig. 1. Fingerprint features at Level 1 (upper row), Level 2 (middle row), and Level 3 (lower row) [3], [4].

endorsed by the forensic community and initiated the establishment of an ANIS/NIST committee, named CDEFFS, to define an extended fingerprint feature set [11]. To our knowledge, this is the first attempt to quantify some of the Level 3 features that are being defined in the "extended feature set" for fingerprint matching [12].

The rest of the paper is organized as follows: Section 2 gives a brief introduction to the history of fingerprint identification, the formation of fingerprints, and the fingerprint sensing technology. Section 3 summarizes previous work done in the domain of automatic fingerprint matching using Level 3 features. Section 4 introduces the proposed automatic feature extraction algorithms for Level 3 features, namely, pores and ridge contours. Section 5 describes in detail the proposed hierarchical matching system with an emphasis on Level 3 matching. Experimental results are provided in Section 6, with summary and future work presented in Section 7.

2 BACKGROUND

2.1 History of Fingerprint Identification

The history of using fingerprints as a scientific method for identification traces back to the 1880s, when Faulds suggested that latent fingerprints obtained at crime scenes could provide knowledge about the identity of offenders [7]. In 1892, Galton published the well-known book entitled *Fingerprints*, in which he discussed the basis of contemporary fingerprint science, including persistence, uniqueness, and classification of fingerprints [13]. Galton introduced Level 2 features by defining minutia points as either ridge endings or ridge bifurcations on a local ridge. He also developed a probabilistic model using minutia points to quantify the uniqueness of fingerprints [13]. Although Galton discovered that sweat pores can also be observed on the ridges, no method was proposed to utilize pores for identification.

In 1912, Locard introduced the science of poroscopy, the comparison of sweat pores for the purpose of personal identification [14]. Locard stated that like the ridge characteristics, the pores are also permanent, immutable, and unique, and are useful for establishing the identity, especially when a sufficient number of ridges is not available. Locard further studied the variation of sweat pores and proposed four criteria that can be used for pore-based identification: the size of the pores, the form of the pores, the position of the pores on the ridges, and the number or frequency of the pores [15]. It was observed that the number of pores along a centimeter of ridge varies from 9 to 18, or 23 to 45 pores per inch and 20 to 40 pores should be sufficient to determine the identity of a person [7]. In particular, pores provide essential information for fragmentary latent print examination since the number of minutia points in latent fragment prints is often too few. One such example is given in Fig. 2, where only one minutia is present in each fragmentary fingerprint, yet the attributes of about
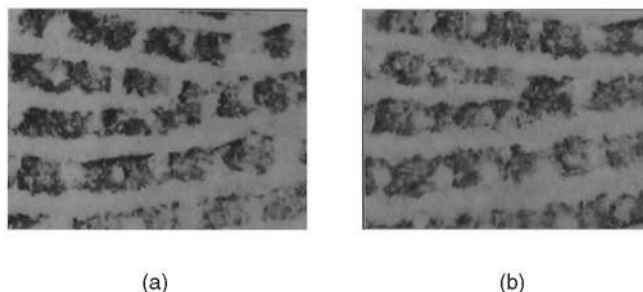
(a)   (b)

Fig. 2. Role of pores in fragmentary latent print examination. (a) and (b) are fingerprint segments from different fingers. The two figures show a bifurcation at the same location on similar patterns. Normal examination would find them in agreement, but their relative pore locations differ (adopted from [7]).
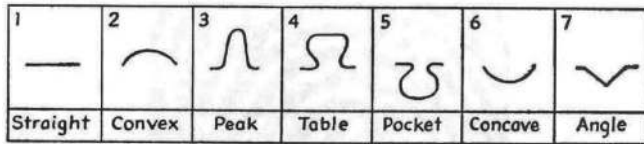
Fig. 3. Characteristic features of friction ridges (adopted from [7]).

20 pores in these images are sufficient to successfully determine a disagreement (nonmatch) between the two prints.

In 1962, Chatterjee proposed the use of ridge edges in combination with other friction ridge formations to establish individualization, which is referred to as "edgeoscopy" [7]. Chatterjee discovered that some shapes on the friction ridge edges tend to reappear frequently and classified them into eight categories, namely, straight, convex, peak, table, pocket, concave, angle, and others (see Fig. 3). Subsequent research established that all the edge characteristics along friction ridges can be placed into one of these categories. It is believed that the differences in edge shapes are caused by the effects of differential growth on the ridge itself or a pore that is located near the edge of the friction ridge. In theory, the density of ridge edge features can be very large, e.g., given the average width of a ridge to be approximately 0.48 mm, a ridge 5 mm long would contain approximately 20 edge characteristics. However, in practice, the flexibility of the friction skin tends to mask all but the largest edge shapes [7].

Over the last 10 years, poroscopy and edgeoscopy have received growing attention and have been widely studied by scientists of ridgeology, a fundamental and essential resource for latent print examiners [7]. It has been claimed that shapes and relative positions of sweat pores and shapes of ridge edges are as permanent and unique as traditional minutia points. And when understood, they add considerable weight to the conclusion of identification [7].

2.2 Fingerprint Formation

Human fingers are known to display friction ridge skin (FRS) that consists of a series of ridges and furrows, generally referred to as fingerprints. The FRS is made of two major layers: dermis (inner layer) and epidermis (outer layer). The ridges emerge on the epidermis to increase the friction between the volar (hand or foot) and the contact surface (see Fig. 4a). A typical young male has, on an average, 20.7 ridges per centimeter while a female has 23.4 ridges per centimeter.

It is suggested that friction ridges are composed of small "ridge units," each with a pore, and the number of ridge units and their locations on the ridge are randomly established. As a result, the shape, size, alignment of ridge units, and their fusion with an adjacent ridge unit are unique for each person. Although there exist certain cases when ridge units fail to compose a ridge, also known as dysplasia, independent ridge units still exist on the skin [7].

Pores, on the other hand, penetrate into the dermis starting from the epidermis. They are defined as the openings of subcutaneous sweat glands that are placed on epidermis. The study in [16] showed that the first sweat gland formations are observed in the fifth month of gestation while the epidermal ridges are not constructed until the sixth month. This implies that the pores are stabilized on the ridges before the process of epidermis and dermis development is completed, and are immutable once the ridge formation is completed. Due to the fact that, each ridge unit contains one sweat gland, pores are often considered evenly distributed along ridges and the spatial distance between pores frequently appears to be in proportion to the breadth of the ridge, which, on an average, is approximately 0.48 mm [7]. A pore can be visualized as either open or closed in a fingerprint image based on its perspiration activity. A closed pore is entirely enclosed by a ridge, while an open pore intersects with the valley lying between two ridges (see Fig. 5). One should not expect to find two separate prints of the same pore to be exactly alike, as a pore may be open in one and closed in the other print.

Occasionally, narrow and often fragmented ridges, also known as incipient ridges, may appear between normal friction ridges. It has been suggested that incipient ridges are normal forming ridges that remained "immature" at the time of differentiation when primary ridge formation stopped. Because pores are formed during the early growth of the ridges, it is observed that some incipient ridges also have pore formations [17]. It has also been observed that incipient ridges occur in about 45 percent of the people and 13.5 percent of the fingers [4]. The incipient ridges are also permanent and repeatable friction ridge characteristics.

A recent study on the microcirculation of human fingers reveals the complexity and characteristics of fingerprints from a microvascular point of view. It has been found that the regular disposition of capillaries on the palmar side of a finger "sharply followed the cutaneous sulci of the fingerprint, reproducing an identical *vascular fingerprint* with the same individual architecture of the cutaneous area" (see Fig. 4b).
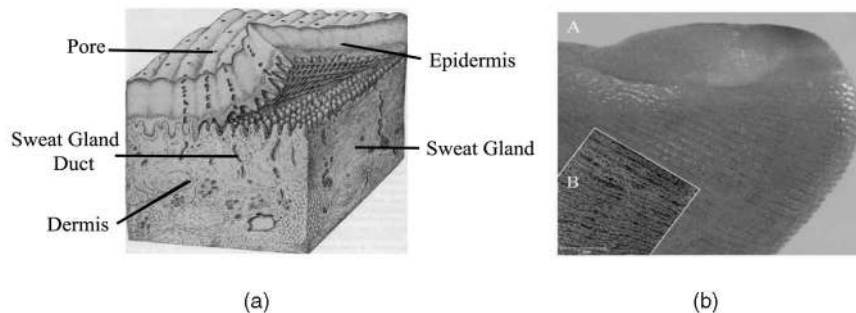

(a)

(b)

Fig. 4. Friction ridge skin. (a) A three-dimensional representation of the structure of ridged skin. The epidermis is partly lifted from the dermis, to expose the dermal papillae (adopted from [2]). (b) A finger seen during the maceration process shows (A) the linear disposition of vessels along the fingerprints and (B) superimposition of a scanning electron microscopy (SEM) image of the same area, revealing perfect correspondence with the fingerprints (adopted from [18]).
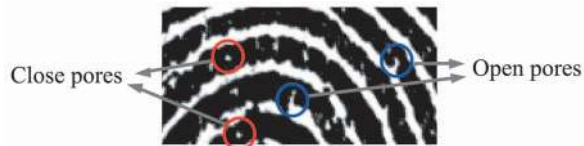
Fig. 5. Open and closed pores in a 1,000 ppi live-scan fingerprint image obtained using a CrossMatch 1000ID sensor.

The capillaries around the sweat glands also formed a very specialized tubular-shaped structure and the concentration of these structures decreases from the palmar to the dorsal side of the finger [18]. This study provides further scientific evidence of the uniqueness of fingerprints.

2.3   Fingerprint Sensing Technology

There are many different sensing methods to obtain the ridge-and-valley pattern of finger skin or fingerprint [19]. Historically, in law enforcement applications, fingerprints were mainly acquired offline. Nowadays, most commercial and forensic applications accept live-scan digital images acquired by directly sensing the finger surface with a fingerprint sensor based on optical, solid-state, ultrasonic, and other imaging technologies.

The earliest known images of fingerprints were impressions in clay and later in wax (see Fig. 2.3 in [7]). Starting in the late 19th century and throughout the 20th century, the acquisition of fingerprint images was mainly performed by using the so-called "ink-technique:" the subject's finger is coated with black ink and pressed and rolled against a paper card; the card was then scanned, producing the digital image. This kind of process is referred to as rolled offline fingerprint sensing, which is still being used in forensic applications and background checks of applicants for sensitive jobs.

Direct sensing of fingerprints as electronic signals started with optical "live-scan" sensors with Frustrated Total Internal Reflection (FTIR) principle. When the finger touches the top side of a glass prism, one side of the prism is illuminated through a diffused light. While the fingerprint valleys that do not touch the glass platen reflect the light, ridges that touch the platen absorb the light. This differential property of light reflection allows the ridges (which appear dark) to be discriminated from the valleys.

Solid-state fingerprint sensing technique uses silicon-based, direct contact sensors to convert the physical information of a fingerprint into electrical signals. The solid-state sensors are based on capacitance, thermal, electric field, radio frequency (RF), and other principles. The capacitive sensor consists of an integrated two-dimensional array of metal electrodes. Each metal electrode acts as one capacitor plate and the contacting finger acts as the second plate. A passivation layer on the surface of the device forms the dielectric between these two plates. A finger pressed against the sensor creates varying capacitance values across the array which are then converted into an image of the fingerprint. Some solid-state sensors can deal with nonideal skin conditions (wet or dry fingers) and are suited for use in a wide range of climates. However, the surface of solid-state sensors needs to be cleaned regularly to prevent the grease and dirt from compromising the image quality.

New fingerprint sensing technologies are constantly being explored and developed. For example, Multispectral Fingerprint Imaging (MSI) has been introduced by Lumidigm, Inc. [20]. Unlike conventional optical fingerprint sensors, MSI devices scan the subsurface of the skin by using different wavelengths of light (e.g., 470 nm (blue), 574 nm (green), and 636 nm (red)). The fundamental idea is that different features of skin cause different absorbing and scattering actions depending on the wavelength of light. Fingerprint images acquired using the MSI technology appear to be of significantly better quality compared to conventional optical sensors for dry and wet fingers. Multispectral fingerprint images have also been shown to be useful for spoof detection [21]. Another new fingerprint sensing technology based on multicamera system, known as "touchless imaging," has been introduced by TBS, Inc. [22]. As suggested by the name, touchless imaging avoids direct contact between the sensor and the skin and, thus, consistently preserves the fingerprint "ground truth" without introducing skin deformation during image acquisition. A touchless fingerprint sensing device is also available from Mitsubishi [23].

One of the most essential characteristics of a digital fingerprint image is its resolution, which indicates the number of dots or pixels per inch (ppi) (see Fig. 6). Generally, 250 to 300 ppi is the minimum resolution that allows the feature extraction algorithms to locate minutiae in a fingerprint image. FBI-compliant sensors must satisfy the 500 ppi resolution requirement. However, in order to capture pores in a fingerprint image, a significantly higher resolution ($\geq$ 1,000 ppi) of image is needed. Although it is not yet practical to design solid-state sensors with such a high resolution due to the cost factor, optical sensors with a resolution of 1,000 ppi are already commercially available. More excitingly, optical sensors with resolutions of 4,000-7,000 ppi are being developed (see Fig. 7), which not only allow capturing Level 3 features for identification, but also pore activities (opening and closing) for spoof detection.
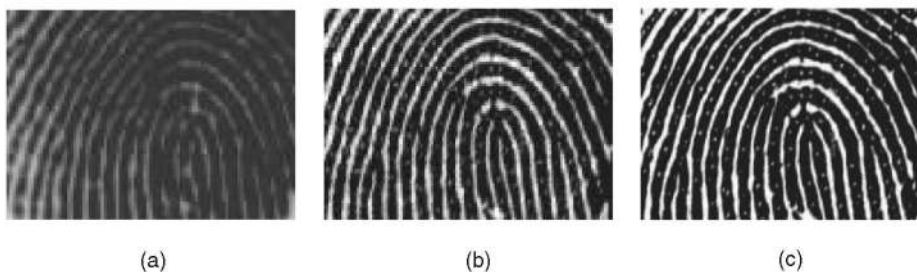

(a)   (b)   (c)

Fig. 6. Fingerprint image resolution. The same fingerprint captured at three different image resolutions (a) 380 ppi (Identix 200DFR), (b) 500 ppi (CrossMatch ID1000), and (c) 1,000 ppi (CrossMatch ID1000).
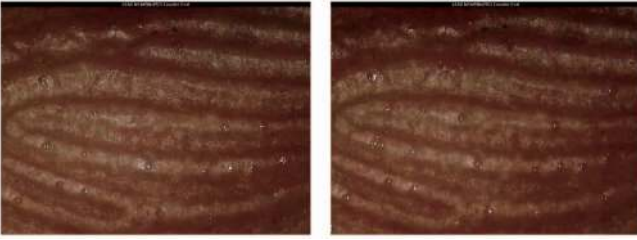
Fig. 7. Two consecutive touchless fingerprint images from a video sequence captured using a very high resolution sensor ($\approx$ 7,000 ppi). The perspiration activities of the pores are clearly seen. (courtesy: TBS (http://www.tbsinc.com/)).

Fig. 9. Pore detection in fingerprint fragments. (a) Detection of open pores. (b) Extraction of open pores (in white) and closed pores (in black) (adopted from [25]).

$$S_p = \left(\sum_{i=0}^{N_s-1} N_{MP,i} \right) / \left(\sum_{i=0}^{N_s-1} N_{P,i} \right), \qquad (1)$$

where N_s is the total number of regions in the template, $N_{P,i}$ is the number of pores detected in template region i, and $N_{MP,i}$ is the number of matching pores in region i. Note alignment is first established based on maximum intensity correlation and two pores are considered matched if they lie within a certain bounding box. Finally, experimental results based on a database of 258 fingerprints from 137 individuals showed that by combining minutia and pore information, a lower FRR of 6.96 percent (compared to $\sim$ 31 percent for minutiae alone) can be achieved at a FAR of 0.04 percent [6].

Based on the above algorithm, Roddy and Stosz [24] later conducted a statistical analysis of pores and presented a model to predict the performance of a pore-based automated fingerprint system. One of the most important contributions of this study is that it mathematically demonstrated the uniqueness of pores, for example, 1) the probability of two consecutive intraridge pores having the same relative spatial position with another two pores is 0.04, 2) the probability of occurrence of a particular combination of 20 consecutive intraridge pores is 1.16×10^{-14}, and 3) the probability of occurrence of a particular combination of 20 ridge-independent pores is 5.186×10^{-8}. In general, this study provides statistics about pores and demonstrates the efficacy of using pores, in addition to minutiae, for improving the fingerprint recognition performance.

More recently, Kryszczuk et al. [25] studied matching fragmentary fingerprints using minutiae and pores. The authors presented two hypotheses pertaining to Level 3 features: 1) the benefit of using Level 3 features increases as the fingerprint fragment size, or the number of minutiae decreases, and 2) given a sufficiently high resolution, the discriminative information contained in a small fragment is no less than that in the entire fingerprint image. Further, Kryszczuk et al. point out that there exists an intrinsic link between the information content of ridge structure, minutiae and pores. As a result, the anatomical constraint that the distribution of pores should follow the ridge structure is imposed in their pore extraction algorithm, which is also based on skeletonization. Specifically, an open pore is only identified in a skeleton image when distance from an end point to a branch point on the valley is small enough (see Fig. 9). Finally, an algorithm based on the geometric distance was employed for pore matching.
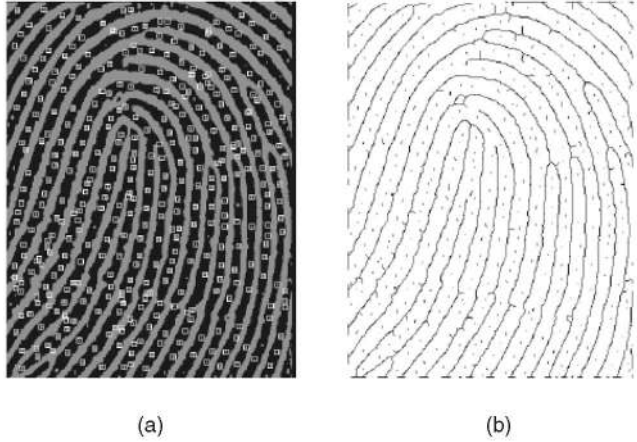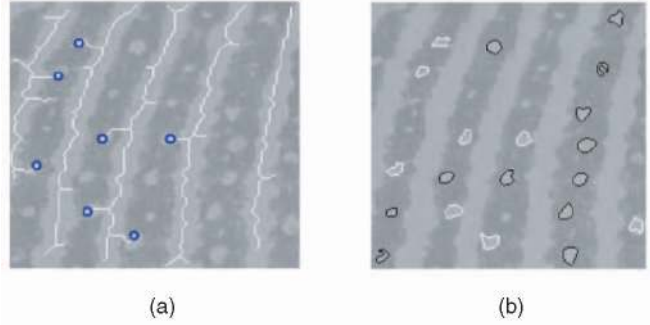

Fig. 8. Pore detection based on skeletonization. (a) A fingerprint image (2,000 ppi) with detected pores (in square boxes). (b) The raw skeleton image, where end points and branch points are tracked for pore extraction (adopted from [6]).

3 PREVIOUS WORK

The use of Level 3 features in an automated fingerprint identification system has been studied by only a few researchers. Existing literature is exclusively focused on the extraction of pores in order to establish the viability of using pores in high resolution fingerprint images to assist in fingerprint identification.

Stosz and Alyea [6] proposed a skeletonization-based pore extraction and matching algorithm [6]. Specifically, the locations of all end points (with at most one neighbor) and branch points (with exactly three neighbors) in the skeleton image are extracted and each end point is used as a starting location for tracking the skeleton. The tracking algorithm advances one element at a time until one of the following stopping criteria is encountered: 1) another end point is detected, 2) a branch point is detected, and 3) the path length exceeds a maximum allowed value. Condition 1) implies that the tracked segment is a closed pore, while Condition 2) implies an open pore. Finally, skeleton artifacts resulting from scars and wrinkles are corrected and pores from reconnected skeletons are removed. The result of pore extraction is shown in Fig. 8. During matching, a fingerprint image is first segmented into small regions and those that contain characteristic features, such as core and delta points, are selected. The match score between a given image pair is then defined as a ratio of the number of matched pores to the total number of pores extracted from template regions,
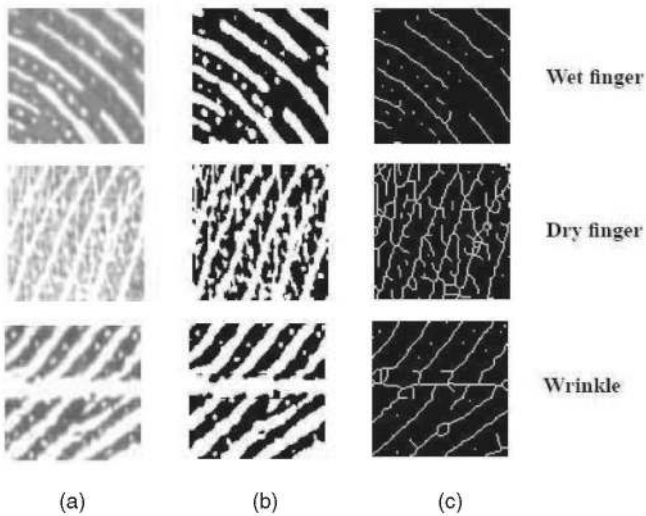
Fig. 10. The sensitivity of skeletonization to various skin conditions and noise. Effects of degradation on (a) gray scale, (b) binary and (c) raw skeleton images are observed for three different sources of noise (adopted from [6]).

Although the hypotheses in previous studies by Stosz et al. [6], [24] and Kryszczuk et al. [25] are well supported by the results of their pilot experiments, there are some major limitations in their approaches:

1. Skeletonization is effective for pore extraction only when the image quality is very good. As the image resolution decreases or the skin condition is not favorable, this method does not give reliable results (see Fig. 10).
2. Comparison of small fingerprint regions based on the distribution of pores requires the selection of characteristic fingerprint segments; which was performed manually in [6].

3. The alignment of the test and the query region is established based on intensity correlation, which is computationally expensive by searching through all possible rotations and displacements. The presence of nonlinear distortion and noise, even in small regions, can also significantly reduce the correlation value.
4. Only custom built optical sensors ($\sim 2,000$ ppi), rather than commercially available live-scan sensors (1,000 ppi) were used in these studies.
5. The database is generally small (e.g., only 12 genuine and six impostor comparisons in [25]).

We propose a fingerprint matching system that is based on 1,000 ppi fingerprint images, acquired using CrossMatch 1000ID, a commercial optical live-scan device. In addition to pores and minutiae, ridge contours that contain discriminatory information are also extracted in our algorithm. We introduce a complete and fully automatic matching framework by efficiently utilizing features at all three levels in a hierarchical fashion. Our matching system works in a more realistic scenario and we demonstrate that inclusion of Level 3 features leads to more accurate fingerprint matching.

4 LEVEL 3 FEATURE EXTRACTION

As suggested in [25], Level 1, Level 2, and Level 3 features in a fingerprint image are mutually correlated. For example, the distribution of pores is not random, but naturally follows the structure of ridges [24]. Also, based on the physiology of the fingerprint, pores are only present on the ridges, not in the valleys. Therefore, it is essential that we identify the location of ridges prior to the extraction of pores. Besides pores, ridge contours are also considered as Level 3 information. During image acquisition, we observe that the ridge contour is often more reliably preserved at 1,000 ppi than the pores, especially in the presence of various skin conditions and sensor noise (see Fig. 11). In

Fig. 11. Two impressions of the same finger at 1,000 ppi. It is observed here that ridge contours are more reliable Level 3 features, compared to pores.
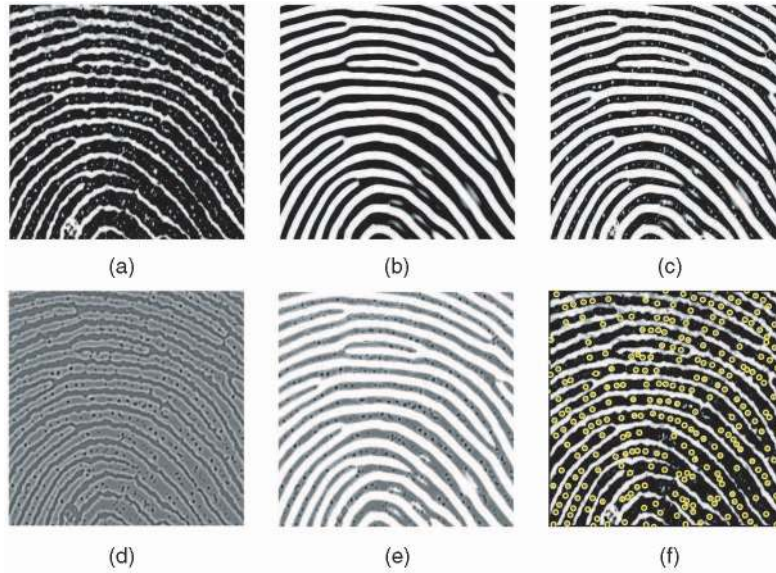
Fig. 12. Pore extraction. (a) A partial fingerprint image at 1,000 ppi. (b) Enhancement of ridges in the image shown in (a) using Gabor filters. (c) A linear combination of (a) and (b). (d) Wavelet response ($s = 1.32$) of the image in (a). (e) A linear combination of (d) and (b). (f) Extracted pores (red circles) after thresholding the image in (e).

order to automatically extract Level 3 features, namely, pores and ridge contours, we have developed feature extraction algorithms using Gabor filters and wavelet transform.

4.1 Pore Detection

Based on their positions on the ridges, pores can be divided into two categories: open and closed. A closed pore is entirely enclosed by a ridge, while an open pore intersects with the valley lying between the two ridges. However, it is not useful to distinguish between the two states for matching since a pore may be open in one image and closed in the other image, depending on the perspiration activity. One common property of pores in a fingerprint image is that they are all naturally distributed along the friction ridge. As long as the ridges are identified, the locations of pores are also determined, regardless of their being open or closed.

To enhance the ridges, we use Gabor filters [26], which has the form

$$G(x, y : \theta, f) = \exp\left\{-\frac{1}{2}\left[\frac{x_\theta^2}{\delta_x^2} + \frac{y_\theta^2}{\delta_y^2}\right] \cos(2\pi f x_\theta)\right\}, \quad (2)$$

where θ and f are the orientation and frequency of the filter, respectively, δ_x and δ_y are the standard deviations of the Gaussian envelope along the x- and y-axes, respectively. Here, (x_θ, y_θ) represents the position of a point (x, y) after it has undergone a clockwise rotation by an angle $(90° - \theta)$. The four parameters $(\theta, f, \delta_x, \delta_y)$ of the Gabor filter are empirically determined based on the ridge frequency and orientation of the fingerprint image [26]. An example of enhanced fingerprint image after Gabor filtering is shown in Fig. 12b. It is clear that ridges are well separated from the valleys after enhancement.

The above procedure suppresses noise by filling all the holes (or pores) on the ridges and highlights only the ridges.

By simply adding it to the original fingerprint image, we observe that both open and closed pores are retained as they appear only on the ridges (see Fig. 12c). However, the contrast between pores and ridges is low in Fig. 12c. In order to enhance the original image with respect to pores, we employ a band pass filter to capture the high negative frequency response as intensity values change abruptly from white to black at the pores. Wavelet transform is known for its highly localized property in both frequency and spatial domains. Hence, we apply the Mexican hat wavelet transform [27] to the input image $f(x, y) \in R^2$ to obtain the frequency response w as follows:

$$w(s, a, b) = \frac{1}{\sqrt{s}} \int \int_{R^2} f(x, y)\phi\left(\frac{x - a}{s}, \frac{y - b}{s}\right) dx dy, \quad (3)$$

where s is the scale factor $(= 1.32)$ and (a, b) are the shifting parameters. Essentially, this wavelet is a band pass filter with scale s. After normalizing the filter response (0-255) using min-max normalization, pore regions that typically have high negative frequency response are represented by small blobs with low intensities (see Fig. 12d). By adding the responses of Gabor and wavelet filters, we obtain the "optimal" enhancement of pores while enforcing the constraint that pores lie only on the ridges (see Fig. 12e). Finally, an empirically determined threshold $(= 58)$ is applied to extract pores with blob size less than 40 pixels. An example of pore extraction is shown in Fig. 12f, where $\sim$ 250 pores, both open and closed, are accurately extracted along the ridges.

Note that our proposed pore extraction algorithm is simple and more efficient than the commonly used skeletonization-based algorithm, which is often tedious and sensitive to noise, especially when the image quality is poor.

4.2 Ridge Contour Extraction

As pointed out earlier, while pores are visible in 1,000 ppi fingerprint images, their presence is not consistent (see
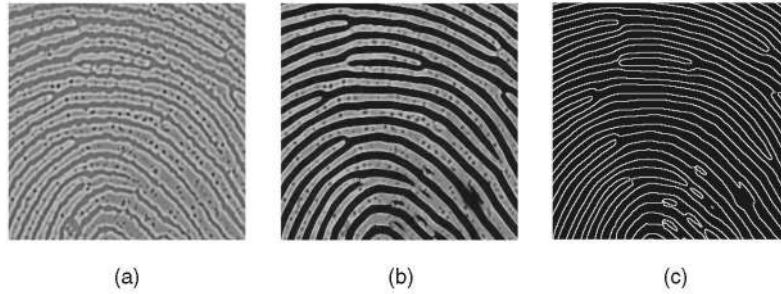
Fig. 13. Ridge contour extraction. (a) Wavelet response (s = 1.74) of the image in Fig. 12a. (b) Ridge contour enhancement using a linear subtraction of wavelet response in (a) and Gabor enhanced image in Fig. 12b. (c) Extracted ridge contours after binarizing (b) and convolving with filter H.

Fig. 11). On the other hand, ridge contours, which contain valuable Level 3 information including ridge width and edge shape, are observed to be more reliable features than pores. Hence, we also extract ridge contours for the purpose of matching.

The ridge contour is defined as edges of a ridge. However, there is a fundamental difference between the use of ridge contours and what is proposed in "edgeoscopy" [7]. In "edgeoscopy," the edge of a ridge is classified into seven categories as shown in Fig. 3. In practice, however, the flexibility of the friction skin and the presence of open pores tend to reduce the reliability of ridge edge classification. In contrast to edgeoscopy, our method utilizes the ridge contour directly as a spatial attribute of the ridge and the matching is based on the spatial distance between points on the ridge contours. Classical edge detection algorithms can be applied to fingerprint images to extract the ridge contours. However, the detected edges are often very noisy due to the sensitivity of the edge detector to the presence of creases and pores. Hence, we again use wavelets to enhance the ridge contours and linearly combine them with a Gabor enhanced image (where broken ridges are fixed) to obtain enhanced ridge contours.

The algorithm to extract ridge contours can be described as follows: First, the image is enhanced using Gabor filters as in (2). Then, we apply a wavelet transform to the fingerprint image to enhance ridge edges (see Fig. 13a). It needs to be noted that the scale s in (3) is now increased to 1.74 in order to accommodate the intensity variation of ridge contours. The wavelet response is subtracted from the Gabor enhanced image such that ridge contours are further enhanced (see Fig. 13b). The resulting image is binarized using an empirically defined threshold $\delta(=10)$. Finally, ridge contours can be extracted by convolving the binarized image $f^b(x,y)$ with a filter H, given by

$$r(x,y) = \Sigma_{n,m} f^b(x,y) H(x-n,y-m), \qquad (4)$$

where filter $H = (0,1,0;1,0,1;0,1,0)$ counts the number of neighborhood edge points for each pixel. A point (x,y) is classified as a ridge contour point if $r(x,y) = 1$ or 2. Fig. 13c shows the extracted ridge contours.

5   HIERARCHICAL MATCHING AND FUSION

In latent print comparison, a forensic expert often investigates Level 3 details when Level 1 or Level 2 features are similar between the template and the query. That is, experts take advantage of an extended feature set in order to conduct a more effective latent matching. A possible improvement of current AFIS systems is then to employ a similar hierarchical matching scheme, which enables the use of an extended feature set for matching at a higher level to achieve robust matching decisions.

Fig. 14 illustrates the architectural design of our proposed matching system. Each layer in the system utilizes features at the corresponding level. All the features that are used in the system are shown in Fig. 15.

Given two fingerprint images, the system first extracts Level 1 (orientation field) and Level 2 (minutiae) features and establishes alignment of the two images using a string-matching algorithm [28]. Agreement between orientation fields of the two images is then calculated using dot-product. If orientation fields disagree $(S_1 < t_1)$, the matcher rejects the query and stops at Level 1. Otherwise, the matcher proceeds to Level 2, where minutia correspondences are established using bounding boxes and the match score S_2 is computed as

$$S_2 = w_1 \times S_1 + w_2 \times \frac{1}{2}$$
$$\left(\frac{N_2^{TQ} - 0.20 \times (N_2^T - N_2^{TQ})}{N_2^T + 1} + \frac{N_2^{TQ} - 0.20 \times (N_2^Q - N_2^{TQ})}{N_2^Q + 1} \right),$$

where w_1 and w_2 $(= 1 - w_1)$ are the weights for combining information at Level 1 and Level 2, N_2^{TQ} is the number of matched minutiae and N_2^T and N_2^Q are the number of minutiae within the overlapping region of the template (T) and the query (Q), respectively. Note that we require $0 \le S_2 \le 100$. Next, we set the threshold t_2 to be 12, such that if $N_2^{TQ} > 12$, the matching terminates at Level 2 and the final match score remains as S_2. Otherwise, we continue investigating Level 3 features. The threshold t_2 is chosen based on the 12-point guideline that is considered as sufficient evidence for making positive identification in many courts of law [5].

As the matching proceeds to Level 3, the matched minutiae at Level 2 are further examined in the context of neighboring Level 3 features. For example, given a pair of matched
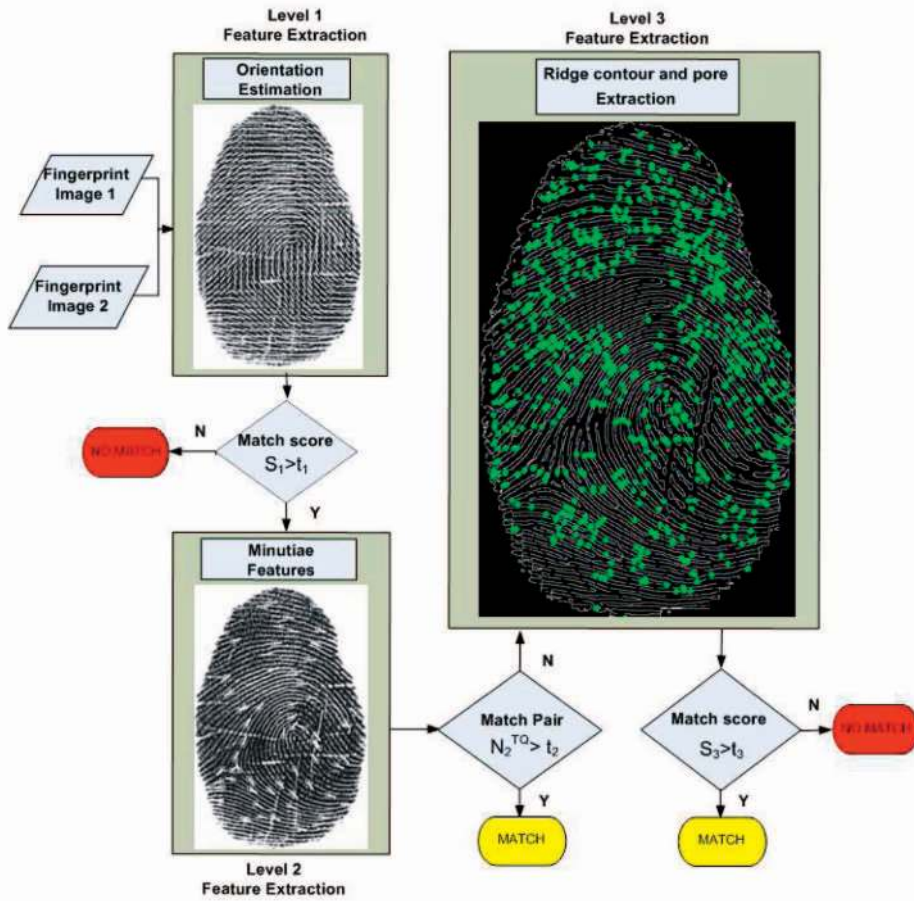
Fig. 14. Hierarchical matching system flow chart. Fingerprint features at three different levels were utilized in a hierarchical fashion.
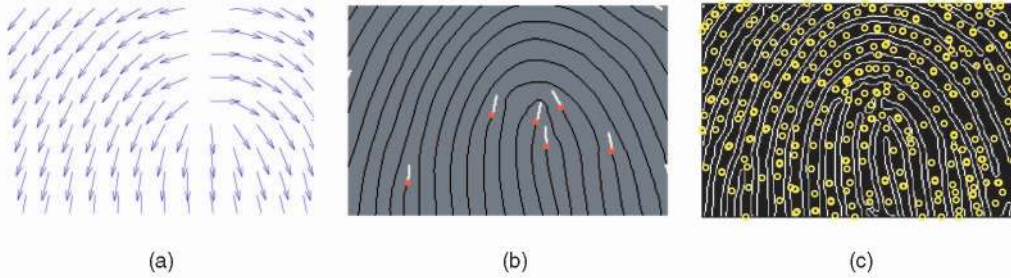

Fig. 15. Different levels of fingerprint features detected in Fig. 6c. (a) Orientation field (Level 1), (b) minutia points (Level 2), and (c) pores and ridge contours (Level 3).

minutiae, we compare Level 3 features in the neighborhood and recompute the correspondence based on the agreement of Level 3 features. Assume an alignment has been established at Level 2, let $(x_i, y_i), i = 1, 2, \ldots, N_2^{TQ}$ be the location of the ith matched minutia and $(\bar{x}, \bar{y})$ be the mean location of all matched minutiae. The associated region of each matched minutia (x_i, y_i) is defined as a rectangular window R_i with size 60×120, centered at $(\frac{x_i + \bar{x}}{2}, \frac{y_i + \bar{y}}{2})$. Note that it is possible for the minutiae to be outside of its associated region, but the selection ensures a sufficiently large foreground region for Level 3 feature extraction. To compare Level 3 features in each local region, we need to take into consideration the fact that the numbers of detected features (pores and ridge contour points), in practice, will be different between query and template, due to degradation of image quality (e.g., skin

deformation). The Iterative Closest Point (ICP) algorithm [29] is a good solution for this problem because it aims to minimize the distances between points in one image to geometric entities (as opposed to points) in the other without requiring 1:1 correspondence. Another advantage of ICP is that when applied locally, it provides alignment correction to compensate for nonlinear deformation [30], assuming that the initial estimate of the transformation is reasonable.

For each matched minutia set $(x_i, y_i), i = 1, 2, \ldots, N_2^{TQ}$, we define its associated regions from T and Q to be R_i^T and R_i^Q, respectively, and the extracted Level 3 feature sets $P_i^T = (a_{i,j}, b_{i,j}, t_{i,j}), j = 1, 2, \ldots N_{3,i}^T$ and $P_i^Q = (a_{i,k}, b_{i,k}, t_{i,k})$, $k = 1, 2, \ldots N_{3,i}^Q$, accordingly. Each feature set includes triplets representing the location of each feature point and its type (pore or ridge contour point). Note that we

avoid matching pores with ridge contour points. The details of matching each Level 3 feature set P_i^T and P_i^Q using the ICP algorithm (see Fig. 16) are given below:

1. Initialize iteration index $k = 0$;

2. Initialize $P_i^{T,0} = P_i^T$ and rigid transformation $W_i^0 = I$;

3. Initialize convergence indicator $Diff = 10^{10}$;

4. Set the stop criterion for distance $D = 0.03$;

5. Set the stop criterion for iteration $Itr = 15$;

6. While $(Diff > D)$

{

6.1. If $(k \geq Itr)$ break;

6.2. $k = k + 1$;

6.3. Apply W_i^{k-1} to the query: $P_i^{T,k} = W_i^{k-1} P_i^{T,k-1}$;

6.4. For $(j = 1$ to $N_{3,i}^Q)$

{

Find index of the closest point for $(a_{i,j}^Q, b_{i,j}^Q, t_{i,j}^Q)$:

$C^k(j) = argmin_g(d((a_{i,g}^{T,k}, b_{i,g}^{T,k}, t_{i,g}^{T,k}), (a_{i,j}^Q, b_{i,j}^Q, t_{i,j}^Q)))$,

$g = 1, 2, ..., N_{3,i}^T$;

}

6.5. Compute the mean distance between $P_i^{T,k}$ and P_i^Q

$E_i^k(P_i^{T,k}, P_i^Q) =$

$\frac{1}{N_{3,i}^Q} \Sigma_{j=1}^{N_{3,i}^Q} d((a_{i,C^k(j)}^{T,k}, b_{i,C^k(j)}^{T,k}, t_{i,C^k(j)}^{T,k}), (a_{i,j}^Q, b_{i,j}^Q, t_{i,j}^Q))$;

6.6. Obtain new transformation W_i^k that minimizes E_i^k;

6.7. Estimate convergence at iteration k

$Diff = E_i^k(P_i^{T,k}, P_i^Q) - E_i^{k-1}(P_i^{T,k-1}, P_i^Q)$;

}

7. Obtain the match distance $E_i = E_i^k(P_i^{T,k}, P_i^Q)$;

The initial transformation W_i^0 in Step 2 was set equal to the identity matrix I as P_i^T and P_i^Q have been prealigned at Level 2. In Steps 6.4 and 6.5, $d(.,.)$ denotes the Euclidean distance between point sets. Note that ICP requires $N_{3,i}^Q$, the number of Level 3 features in query region R_i^Q, be always smaller than $N_{3,i}^T$, the number of Level 3 features in R_i^T. This can be satisfied by choosing the feature set with the larger size to be the template. Fast convergence of the ICP algorithm is usually assured because the initial alignment based on minutiae at Level 2 is generally good. When the algorithm converges or is terminated when $k = 15$, the match distance E_i is obtained.
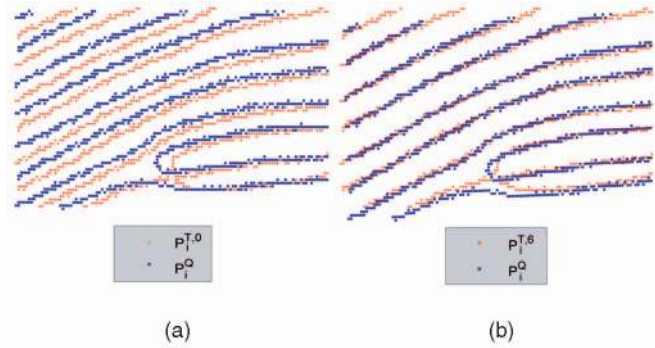

Fig. 16. An example of using the ICP algorithm for Level 3 matching. After $k = 6$ iterations, the mean match distance E_i (per feature point) between P_i^T and P_i^Q is reduced from 3.03 pixels in (a) to 1.18 pixels in (b).
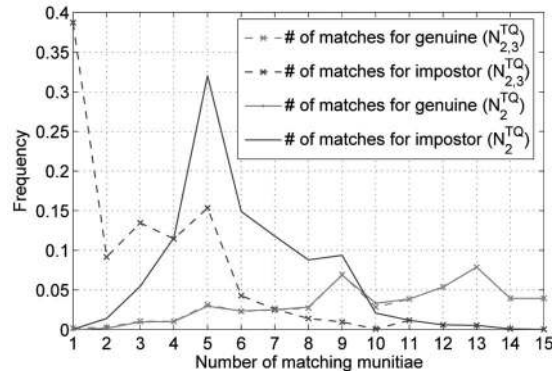

Fig. 17. The advantage of using Level 3 features. Curves corresponding to N_2^{TQ} are based on Level 2 features alone and curves correspond to $N_{2,3}^{TQ}$ are based on Level 2 and Level 3 features. Note that $N_{2,3}^{TQ} \leq N_2^{TQ}$. In general, the number of impostor minutia matches decreases after Level 3 features are used, while the number of genuine minutia matches remains almost unchanged. As a result, the overlap region of the genuine and impostor distributions of matched minutiae is reduced after Level 3 features were utilized.

Given N_2^{TQ} matched minutiae between T and Q at Level 2, N_2^{TQ} match distances $E_i, i = 1, 2, \ldots, N_2^{TQ}$ based on Level 3 features will be obtained using the above algorithm. Each distance E_i is then compared with a threshold t_d and if $E_i < t_d$, the associated minutia correspondence is ensured, otherwise, the correspondence is denied. Let $N_{2,3}^{TQ}$ be the updated number of matched minutiae, $N_{2,3}^{TQ} \leq N_2^{TQ}$ (Fig. 17). The match score S_3 is defined as

$$S_3 = w_1 \times S_1 + w_2 \times \frac{1}{2}$$
$$\left(\frac{N_{2,3}^{TQ} - 0.20 \times (N_2^T - N_{2,3}^{TQ})}{N_2^T + 1} + \frac{N_{2,3}^{TQ} - 0.20 \times (N_2^Q - N_{2,3}^{TQ})}{N_2^Q + 1} \right),$$

where N_2^T and N_2^Q, as before, are the number of minutiae within the overlapped region of the template and the query, respectively. Note that $0 \leq S_3 \leq 100$.

The proposed hierarchical matcher utilizes a fusion scheme that integrates the feature information at Level 2 and Level 3 in a cascade fashion. An alternative approach that integrates match scores at Level 2 and Level 3 in a parallel fashion was also proposed in [31], where min-max normalization and sum rule were employed to fuse the two
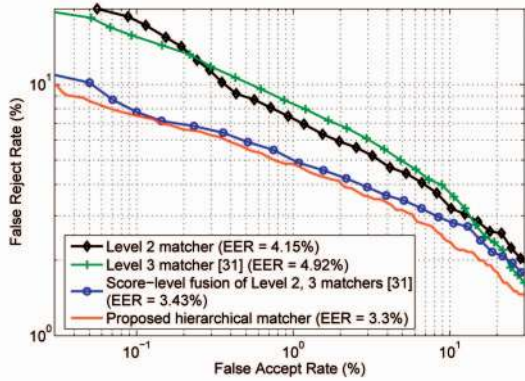
Fig. 18. ROC curves for the individual Level 2 matcher and Level 3 matcher, score-level fusion of both matchers [31] and the proposed hierarchical matcher.
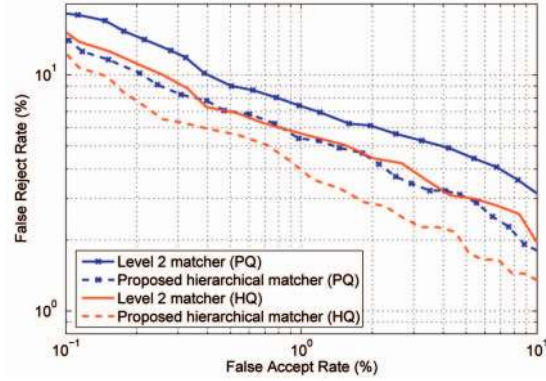
Fig. 19. ROC curves for the Level 2 matcher and the proposed matcher across different quality, namely, high quality (HQ) and low quality (LQ) images.

match scores. Although the latter is a more commonly used and straight-forward approach, it is more time-consuming since matching at both Level 2 and Level 3 has to be performed for every query. In addition, parallel score fusion is sensitive to the selected normalization scheme and fusion rule. On the other hand, the proposed hierarchical matcher enables us to control the level of information or features to be used at different stages of fingerprint matching.

6 EXPERIMENTAL RESULTS

To our knowledge, there is no 1,000 ppi resolution fingerprint database available in the public domain. Hence, we collected our own 1,000 ppi fingerprint database with 410 fingers (41 subjects × 10 fingers per subject) using a CrossMatch 1000ID sensor. Each finger contributed four impressions (2 impressions × 2 sessions with an interval of three days) resulting in 1,640 fingerprint images in our database.

Experiments are carried out to estimate the performance gain of utilizing Level 3 features in a hierarchical matching system, and more importantly, across two different fingerprint image quality types. The average time of feature extraction and matching at Level 3 are ∼ 3.5 seconds per image and ∼ 45 seconds per match, respectively, when tested on a PC with 1GB of RAM and a 1.6GHz Pentium 4 CPU. All programs are currently implemented in MATLAB and we expect the computational costs to be significantly reduced after optimization.

In the first experiment, we compare the matching performance of the proposed hierarchical matcher to that of the individual Level 2 and Level 3 matchers and their score-level fusion [31] across the entire database. For each matcher, the number of genuine and impostor matches are 2,460 (410 × 6) and 83,845 ($\frac{410 \times 409}{2}$), respectively. Note that we exclude symmetric matches of the same pair as well as matches between the same image. As shown in Fig. 18, the proposed hierarchical matcher results in a relative performance gain of ∼ 20 percent in terms of EER over the Level 2 matcher. It also consistently outperforms the score-level fusion of individual Level 2 and Level 3 matchers [31], especially at high FAR values. These results strongly suggest that Level 3 features provide valuable complementary

information to Level 2 features and can significantly improve the current AFIS matching performance when combined with Level 2 features using the proposed hierarchical structure.

In the second experiment, our aim was to test whether the performance gain of the proposed hierarchical matcher is consistently observed across different image quality. We divided the entire database into two equal-sized groups with respect to image quality, namely, high quality (HQ) and low quality (LQ) and applied both Level 2 matcher and the proposed hierarchical matcher to each group exclusively. The average number of genuine and impostor matches for each quality group, respectively, are 820 and 20,961. The fingerprint image quality measure we employ is based on spatial coherence, as proposed in [32]. Note that this quality measure also favors large-sized fingerprints, hence, images with small fingerprint regions are often assigned low quality values. As shown in Fig. 19, consistent performance gain of the proposed hierarchical matcher over the Level 2 matcher is observed across different image quality groups. This result contradicts the general assertion that Level 3 features should only be used when the fingerprint image is of high quality. In fact, high quality fingerprint images typically contain a sufficiently large number of Level 2 features for accurate identification. It is often the fingerprint images with low quality, especially prints of small size (mostly seen in latent prints), that gain the most from matching using Level 3 features.

In general, our experiments show significant performance improvement when we combine Level 2 and Level 3 features in a hierarchical fashion. It is demonstrated that Level 3 features do provide additional discriminative information and should be used in combination with Level 2 features. The results of this study strongly suggest that using Level 3 features in fingerprint matching at 1,000 ppi is both practical and beneficial.

7 SUMMARY AND CONCLUSIONS

We have presented an automated fingerprint matching system that utilizes fingerprint features in 1,000 ppi images

at all three levels. To obtain discriminatory information at Level 3, we introduced algorithms based on Gabor filters and wavelet transform to automatically extract pores and ridge contours. A modified ICP algorithm was employed for matching Level 3 features. Our experimental results demonstrate that Level 3 features should be examined to refine the establishment of minutia correspondences provided at Level 2. More importantly, consistent performance gains were also observed in both high quality and low quality images, suggesting that automatically extracted Level 3 features can be informative and robust, especially when the fingerprint region, or the number of Level 2 features, is small. The potential of improving AFIS matching by utilizing Level 3 features at 1,000 ppi is promising and should be further investigated. Currently, we are in the process of optimizing our algorithm and acquiring a larger database for testing. We are also exploring automatic extraction of additional Level 3 feature types.

ACKNOWLEDGMENTS

REFERENCES

[1]   F. Galton, "Personal Identification and Description," *Nature,* vol. 38, pp. 201-202, 1888.
[2]   H. Cummins and M. Midlo, *Finger Prints, Palms and Soles: An Introduction to Dermatoglyphics.* Dover, 1961.
[3]   "The Thin Blue Line," http://www.policensw.com/info/fingerprints/finger06.html, Oct. 2006.
[4]   H.v.d. Nieuwendijk, "Fingerprints," http://www.xs4all.nl/~dacty/minu.htm, Oct. 2006.
[5]   S. Pankanti, S. Prabhakar, and A.K. Jain, "On the Individuality of Fingerprints," *IEEE Trans. Pattern Analysis and Machine Intelligence,* vol. 24, no. 8, pp. 1010-1025, Aug. 2002.
[6]   J.D. Stosz and L.A. Alyea, "Automated System for Fingerprint Authentication Using Pores and Ridge Structure," *Proc. SPIE Conf. Automatic Systems for the Identification and Inspection of Humans,* vol. 2277, pp. 210-223, 1994.
[7]   D.R. Ashbaugh, *Quantitative-Qualitative Friction Ridge Analysis: An Introduction to Basic and Advanced Ridgeology.* CRC Press, 1999.
[8]   J. Thornton, "Latent Fingerprints, Setting Standards in the Comparison and Identification," *Proc. 84th Ann. Training Conf. Calif. State Division of IAI,* May 2000.
[9]   R. McCabe and M. Garris, "Summary of April 2005 ANSI/NIST Fingerprint Standard Update Workshop," http://fingerprint.nist.gov/standard/, 2005.
[10]   "SWGFAST, Scientific Working Group on Friction Ridge Analysis, Study and Technology," http://www.swgfast.org/, Oct. 2006.
[11]   "CDEFFS: The ANIS/NIST Committee to Define an Extended Fingerprint Feature Set," http://fingerprint.nist.gov/standard/cdeffs/index.html, Oct. 2006.
[12]   S. Meagher and A. Hicklin, "Extended Fingerprint Feature Set," *Proc. ANSI/NIST ITL 1-2000 Standard Update Workshop,* 2005.
[13]   F. Galton, *Fingerprints (reprint).* Da Capo Press, 1965.
[14]   E. Locard, "Les Pores et L'Identification Des Criminels," *Biologica: Revue Scientifique de Medicine,* vol. 2, pp. 357-365, 1912.
[15]   B. Wentworth and H. Wilder, *Personal Identification.* T.G. Cooke, 1932.
[16]   W. Hirsch and J.U. Schweichel, "Morphological Evidence Concerning the Problem of Skin Ridge Formation," *J. Mental Deficiency Research,* vol. 17, no. 1, pp. 58-72, 1973.
[17]   D.R. Ashbaugh, "Incipient Ridges and the Clarity Spectrum," *J. Forensic Identification,* vol. 42, no. 2, p. 106, 1992.
[18]   S. Sangiorgi, A. Manelli, T. Congiu, A. Bini, G. Pilato, M. Reguzzoni, and M. Raspanti, "Microvascularization of the Human Digit as Studied by Corrosion Casting," *J. Anatomy,* vol. 204, pp. 123-131, 2004.
[19]   X. Xia and L. O'Gorman, "Innovations in Fingerprint Capture Devices," *Pattern Recognition,* vol. 36, no. 2, pp. 361-369, 2003.
[20]   R.K. Rowe, S.P. Corcoran, K.A. Nixon, and R.E. Ostrom, "Multi-spectral Imaging for Biometrics," *Proc. SPIE Conf. Spectral Imaging: Instrumentation, Applications, and Analysis,* pp. 90-99, Mar. 2005.
[21]   K.A. Nixon and R.K. Rowe, "Multispectral Fingerprint Imaging for Spoof Detection," *Proc. SPIE Conf. Biometric Technology for Human Identification,* pp. 214-225, Mar. 2005.
[22]   G. Parziale and E. Diaz-Santana, "The Surround Imager: A Multi-Camera Touchless Device to Acquire 3D Rolled-Equivalent Fingerprints," *Proc. Int'l Conf. Biometrics,* pp. 244-250, 2006.
[23]   "Mitsubishi Touchless Fingerprint Sensor," http://global.mitsubishielectric.com, Oct. 2006.
[24]   A.R. Roddy and J.D. Stosz, "Fingerprint Features—Statistical Analysis and System Performance Estimates," *Proc. IEEE,* vol. 85, no. 9, pp. 1390-1421, 1997.
[25]   K. Kryszczuk, A. Drygajlo, and P. Morier, "Extraction of Level 2 and Level 3 Features for Fragmentary Fingerprints," *Proc. Second COST Action 275 Workshop,* pp. 83-88, 2004.
[26]   L. Hong, Y. Wan, and A.K. Jain, "Fingerprint Image Enhancement: Algorithms and Performance Evaluation," *IEEE Trans. Pattern Analysis and Machine Intelligence,* vol. 20, no. 8, pp. 777-789, Aug. 1998.
[27]   C. Burrus, R. Gopinath, and H. Guo, *Introduction to Wavelets and Wavelet Transforms.* Prentice Hall, 1998.
[28]   A.K. Jain, S. Prabhakar, and S. Chen, "Combining Multiple Matchers for a High Security Fingerprint Verification System," *Pattern Recognition Letters,* vol. 20, nos. 11-13, pp. 1371-1379, 1999.
[29]   P.J. Besl and N.D. McKay, "A Method for Registration of 3D Shapes," *IEEE Trans. Pattern Analysis and Machine Intelligence,* vol. 14, no. 2, pp. 239-256, Feb. 1992.
[30]   A. Ross, S.C. Dass, and A.K. Jain, "Fingerprint Warping Using Ridge Curve Correspondences," *IEEE Trans. Pattern Analysis and Machine Intelligence,* vol. 28, no. 1, pp. 19-30, Jan. 2006.
[31]   A.K. Jain, Y. Chen, and M. Demirkus, "Pores and Ridges: Fingerprint Matching Using Level 3 Features," *Proc. Int'l Conf. Pattern Recognition,* vol. 4, pp. 477-480 Aug. 2006.
[32]   Y. Chen, S.C. Dass, and A.K. Jain, "Fingerprint Quality Indices for Predicting Authentication Performance," *Proc. Audio- and Video-Based Biometric Person Authentication,* pp. 160-170, 2005.

Anil K. Jain received the BTech degree from the Indian Institute of Technology, Kanpur, and the MS and PhD degrees from The Ohio State University. He is a University Distinguished Professor in the Department of Computer Science and Engineering at Michigan State University. He received a distinguished alumni award from The Ohio State University. His research interests include statistical pattern recognition, data clustering, and biometric authentication. He received the 1996 IEEE Transactions on Neural Networks Outstanding Paper Award and best paper awards from the Pattern Recognition Society in 1987 and 1991. He was the editor-in-chief of the *IEEE Transactions on Pattern Analysis and Machine Intelligence*. He is a fellow of the IEEE, ACM, IAPR, SPIE, and AAAS. He has received a Fulbright Research Award, a Guggenheim fellowship, the Alexander von Humboldt Research Award, and the 2003 IEEE Computer Society Technical Achievement Award. He holds six patents in the area of fingerprint matching and he is the author of a number of books, including the *Handbook of Multibiometrics*, (Springer 2006), *Biometric Systems, Technology, Design, and Performance Evaluation*, (Springer 2005), *Handbook of Face Recognition*, (Springer 2005), *Handbook of Fingerprint Recognition*, (Springer 2003, received the PSP award from the Association of American Publishers), *BIOMETRICS: Personal Identification in Networked Society*, (Kluwer 1999) and *Algorithms for Clustering Data*, (Prentice-Hall 1988). ISI has designated him as a highly cited researcher. He is an associate editor of the *IEEE Transactions on Information Forensics and Security* and *ACM Transactions on Knowledge Discovery in Data*. He is a member of the National Academies panels on Whither Biometrics and Improvised Explosive Device.

Yi Chen received the BS degree in computer science and engineering from Sichuan University, Chengdu, China, in 2002. She is currently enrolled in a dual degree program in computer science and engineering (doctoral) and statistics (masters) at Michigan State University. Her research interests include statistical pattern recognition, image processing, and biometric authentication. She worked as a summer research intern at Identix Corporate Research, New Jersey, and at TBS Holding, Switzerland, in 2005 and 2006, respectively. She is a coauthor of the Motorola Best Student Paper at the International Conference on Biometrics (ICB), Hong Kong, 2006. She is a member of CDEFFS, the ANSI/NIST committee to define an extended fingerprint feature set. She is also a student member of the IEEE.

Meltem Demirkus received the BS degree in computer science and engineering from Isik University, Istanbul, Turkey, in 2004. She is currently a doctoral student in the Department of Computer Science and Engineering, Michigan State University, East Lansing. Her research interests include biometrics, pattern recognition, computer vision, and image processing. She worked as a research intern at Siemens Corporate Research, New Jersey, from 2004 to 2005 and a summer intern at Lumidigm, New Mexico, in 2006, respectively. She is a student member of the IEEE.

▷ **For more information on this or any other computing topic, please visit our Digital Library at** www.computer.org/publications/dlib.